Porosity-Zoned Porous-Transport Layer for Proton-Exchange Membrane Water Electrolysis by High-Velocity Flame Spraying

Kirsten Bobzin, Selina Finger,* Lidong Zhao,* Hendrik Heinemann, Elisa Olesch, Katja Radermacher, Sabrina Pechmann, Dennis Possart, Silke H. Christiansen, Darius Hoffmeister, Birk Fritsch, Simon Thiele, and Andreas Hutzler

The porous-transport layer (PTL) is a crucial component in proton-exchange membrane water electrolyzers (PEMWE) enabling water and gas transport as well as electrically contacting the catalyst layer (CL). To reduce the overall costs of PTLs, a fabrication method by high-velocity oxy-fuel (HVOF) spraying is introduced. Free-standing PTLs are obtained via the application of a titanium coating onto a substrate and its subsequent separation and thermal treatment. The obtained PTLs feature two sides of different roughness and porosity as analyzed and visualized by X-ray microscopy. This way, the side with decreased porosity (21%) is intended to function as a microporous layer, improving the contact with the CL. The presented fabrication process promises decreased costs compared to vacuum plasma spraying, a simplified, chemical-free mechanical separation of the PTL from the substrate, and a high scale-up suitability. In the results, it is demonstrated that HVOF can produce titanium PTLs with low oxygen content. Additionally, PEMWE single-cell tests demonstrate that the sprayed PTLs perform on par with a commercially available PTL material.

1. Introduction

Considering the energy transition needed to tackle climate change, an energy carrier is required to bridge the gap between the supply and demand of inherently fluctuating renewable energies. Hydrogen produced by water splitting is increasingly gaining interest as an energy carrier. Proton-exchange membrane water electrolysis (PEMWE) is one of the most promising technologies for producing green hydrogen due to its high power densities and ability to follow fast load changes.[1]

However, the high costs of PEMWE materials and the component manufacturing processes present a major obstacle to further market expansion.[2–4] Anode-side components especially employ expensive materials to withstand the harsh operation conditions of high electrochemical potentials, low pH environment, and elevated temperatures. The materials of choice are iridium and titanium based, which have been proven to withstand these operation conditions.[2] So far, substantial research efforts aimed at reducing the iridium content in the catalyst layer (CL)[5–8] or replacing titanium as the base material for bipolar plates (BPP) by coated stainless steel.[9,10] For the porous-transport layer (PTL), however, the replacement of titanium seems not viable at this point. A different approach to minimizing costs is urgently needed since 17% of the stack costs account for the PTL.[11] Potential for cost reduction lies in optimizing mass and charge transport to increase PEMWE efficiency and improving the PTL manufacturing process.[2]

Commercial anodic PTLs are produced by sintering titanium powders or fibers and stamping or stretching titanium metal sheets.[4,12] They usually feature a nongraded structure with homogeneous porosities of 30–50%.[12,13] The dominant task at the two interfaces of the PTL differs, resulting in dissimilar structural requirements. At the BPP–PTL interface, fast transport (large pore phase) of reactants and products is needed. The CL–PTL interface, in turn, demands low electrical contact resistance (large contact area) and mechanical support for the membrane and CL.[14,15] In addition, the PTL plays a vital role in the heat management of the cell.[16] Hence, a nongraded PTL structure is always a nonideal compromise.

Improving the CL–PTL interface has gained more attention due to issues arising from decreasing the iridium loadings in the

K. Bobzin, L. Zhao, H. Heinemann, E. Olesch, K. Radermacher
Surface Engineering Institute
RWTH Aachen University
52072 Aachen, Germany
E-mail: zhao@iot.rwth-aachen.de

S. Finger, D. Hoffmeister, B. Fritsch, S. Thiele, A. Hutzler
Forschungszentrum Jülich GmbH
Helmholtz Institute Erlangen-Nürnberg for Renewable Energy (IET-2)
91058 Erlangen, Germany
E-mail: s.finger@fz-juelich.de

S. Finger, D. Hoffmeister, S. Thiele
Department Chemical and Biological Engineering
Friedrich-Alexander-Universität Erlangen-Nürnberg
91058 Erlangen, Germany

S. Pechmann, D. Possart, S. H. Christiansen
Correlative Microscopy
Fraunhofer Institute for Ceramic Technologies and Systems IKTS
91301 Forchheim, Germany

The ORCID identification number(s) for the author(s) of this article can be found under https://doi.org/10.1002/adem.202402462.

**ADVANCED
SCIENCE NEWS**

www.advancedsciencenews.com

**ADVANCED
ENGINEERING
MATERIALS**

www.aem-journal.com

CL.[17] A reduction of the loading involves a decrease in CL thickness. If the CL gets too thin, the in-plane electrical conduction is interrupted. This leads to a performance decrease due to inactive parts of the CL if a PTL with a large pore size is used.[18]

Recent literature examines the impact of PTL structural properties on the PEMWE performance.[15,19–24] For example, PEMWE performance improvements are observed when the pore size or porosity of the PTL is decreased with a lower threshold defined by the PTL structure and mass transport issues.[15,17,19,25] Additionally, membrane deformation is reduced, opening possibilities for decreased membrane thickness and, therefore, reduced ionic resistance and cost.[22]

To balance the demands on the CL–PTL and BPP–PTL interface, pore sizes or porosity throughout the PTL thickness need to be tailored accordingly. Consequently, the manufacturing of graded PTLs is currently intensively investigated.[17,25–28] In this context, modifying the PTL fabrication processes bears the potential for cost reduction.[3,29] In all fabrication processes, a PTL structure with low oxygen content is aimed for due to the need for high electrical conductivity. Manufacturing routes for graded PTL structures include diffusion bonding of two layers with different structures, porosity, and pore size,[25] co-sintering of powders with different properties,[14] or altering PTL surface properties via lasing.[21,30] Additionally, the fabrication of multilayered structures by thermal spraying processes showed promising results.[26,28]

In thermal spraying, powder- or wire-based feedstock materials are heated, molten, or partially molten by a spray gun, accelerated as particles in a gas stream, and impacted onto the surface of the substrate to be coated. Upon contact with the substrate, the particles flatten, solidify, and cool down. Parts of the particles remain attached to the substrate primarily by mechanical interlocking. A roughened substrate surface promotes mechanical interlocking and, thus, coating adhesion because overlapping particles form a coating.[31] PTLs modified or fabricated by a process variant of thermal spraying called vacuum plasma spraying (VPS) showed promising results.[26,28] Modifying the pore structure of a PTL of sintered titanium powder could improve the cell performance and Ohmic resistances, although the PTLs exhibited a low porosity of less than 25%.[26] In addition, free-standing PTLs were fabricated via VPS by chemically detaching the coating from a substrate and showing similar performance compared to sintered material in single-cell tests.[28] VPS takes place in a vacuum chamber, which excludes reactions of feedstock materials with oxygen or nitrogen from the atmosphere.[31] However, the vacuum process increases costs compared to other spray processes. Thus, the spraying of PTLs without vacuum requirements is economically demanded.

In this context, high-velocity oxy-fuel (HVOF) spraying is of great interest. HVOF is a thermal spraying technique in which oxygen and fuel combustion occurs under a high pressure of 4–8 bar with flame temperatures of 2500–3100 °C.[32] The combustion gas expansion through a converging–diverging nozzle enables high gas velocities of more than $2000\,\mathrm{m\,s^{-1}}$. Combined with high gas densities, powder particles injected into the gas stream are accelerated to high velocities, usually between 400 and $800\,\mathrm{m\,s^{-1}}$. The high velocities and more moderate temperatures compared to a plasma torch lead to dense, firmly adhering, and low-oxide metallic or carbide coatings.[31] The lower process costs compared to VPS and the limited oxidation of the metallic materials due to the low melting degrees of metal

powders are favored for PTL fabrication. However, high porosities of PTL generally present a considerable challenge for HVOF due to high particle velocities. There are no reports on the fabrication of titanium PTLs using HVOF yet.

Using spray-coated materials as PTL requires facile and scalable substrate removal. Chemical etching is a possible method to detach the porous structure from the substrate, as reported by Lettenmeier et al.[28] However, this is unsuitable for the scale-up of PTL fabrication due to the high amount of chemical waste. In addition to chemical methods, coatings can also be detached mechanically: NiAl,[33] WC–Co,[34] and ceramic coatings[35] were successfully separated from austenitic steel substrates. These studies, however, do not consider process and cost efficiency concerning a possible large series production of free-standing coatings.

In this study, we demonstrate a feasible PTL fabrication by HVOF. The spray process was adapted to achieve high porosity and minimize the oxidation of titanium. In addition, a method for reproducible mechanical PTL separation was developed. The surface topography, coating structure, oxygen content, and pore structure of the PTLs are studied using confocal laser scanning microscopy (CLSM), scanning electron microscopy (SEM), carrier gas hot extraction, and X-ray microscopy (XRM). Additionally, the impact of heat treatment on the electrical resistance of the PTLs is investigated. Finally, the PTL performance is analyzed using PEMWE single-cell tests, showing that the material is competitive with commercial alternatives.

2. Results and Discussion

2.1. Fabrication of PTLs

PTLs are obtained by HVOF spraying of titanium powder (grade 4) onto a substrate, removal of the coating from the substrate, and subsequent heat treatment of the PTL. The HVOF system uses hydrogen as fuel gas and nitrogen as shielding and carrier gas and is schematically depicted in **Figure 1**a. The advantage of nitrogen as a shielding gas is that the oxidation of the metallic spray powders can be effectively reduced.[36] The spray parameters can be found in Table 2 which resulted from a parameter study done in previous works.[37] The obtained structure is a result of a fine tuning of these spray parameters and highly depends on them.

To obtain free-standing PTLs, the coatings are removed from the substrate. A crucial advancement of our fabrication technique is the simplified mechanical removal of the PTL from the substrate compared to chemical removal in other research.[28] For thermal spraying, substrate surfaces are typically roughened, e.g., by grit blasting, to support mechanical interlocking. In our case, however, the PTL must be removed from the substrate, which is hindered by mechanical interlocking. Therefore, the substrates used to spray onto exhibit an average surface roughness of Ra < 1 μm, determined by CLSM. A decreased roughness is essential for low coating adhesion and, thus, the subsequent mechanical separation. This way, a simple coating separation process is possible, as demonstrated in Figure 1b,c, where the PTL is removed from the substrate by a piece of paper. In addition to reducing chemical usage, a major advantage of mechanical separation is that the substrate remains largely intact. Thus,
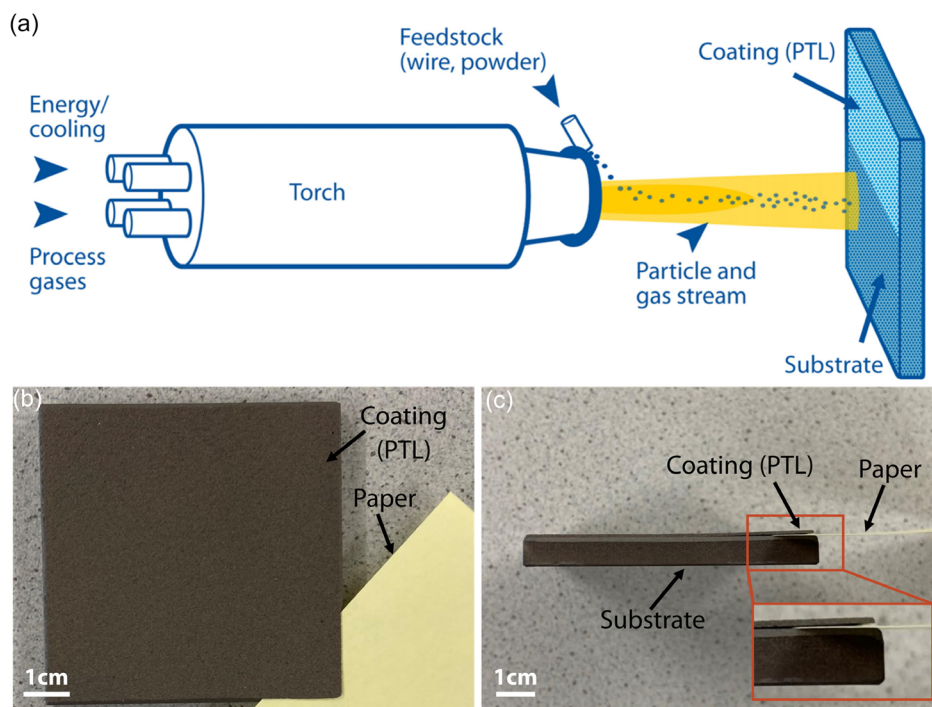
Figure 1. a) Schematic of thermal spraying process adapted from ref. [65]. b,c) Mechanical separation of PTL from the substrate with a piece of paper.

the reusability of the substrate allows the production of more than 20 free-standing PTLs in succession. The easy removal of the sprayed coatings was also proven for two other spray conditions which selected to examine the robustness of this method. When increasing the total gas flow rate to $Q_{O2+H2} = 550$ standard liter per minute (SLPM) as well as increasing the stand-off distance to 170 mm, the titanium coatings can be well separated from the substrate. The mechanical removal with paper is possible for a PTL thickness range of around 200–1000 μm. If the PTLs are significantly thinner than 200 μm, they must be separated with a razor blade because adhesion to the substrate is locally too high for paper. An explanation for this is based on the stresses forming during the thermal spraying process. After thermal spraying, the residual stresses remaining in the titanium layer are the internal driving force for its separation.[38] The strain energy release rate G can be used to estimate the internal driving force. In the simplest case of a layer with uniform strain distribution, G is the stored elastic strain energy per unit interface given by

$$G \approx \frac{\sigma_c^2 s}{2 E_c} \qquad (1)$$

where s is the thickness of the titanium layer, σ_C^2 is the residual stress, and E_c is the Young's modulus of the PTL.[38] The strain energy release rate increases linearly with the square of the residual stress and with the layer thickness. Thus, PTLs significantly thinner than 200 μm are challenging to separate using paper. Given the application of the PTLs in PEMWE single cells, PTLs in a thickness range of 480–520 μm were produced and analyzes in this study.

Our chosen fabrication method yields PTLs with two sides of different morphology, as shown in **Figure 2**. The side of the PTL that was separated from the substrate (called separated side) is flat compared to the rough side where the buildup of the material took place (called buildup side). Furthermore, this leads to a smooth separated side of the free-standing PTL. This unique structure is supposed to be beneficial for PEMWE to improve the interfacial contact with the CL, especially when a porous-transport electrode (PTE) approach is targeted. In the case of a PTE approach, the flat surface would be coated with catalyst,
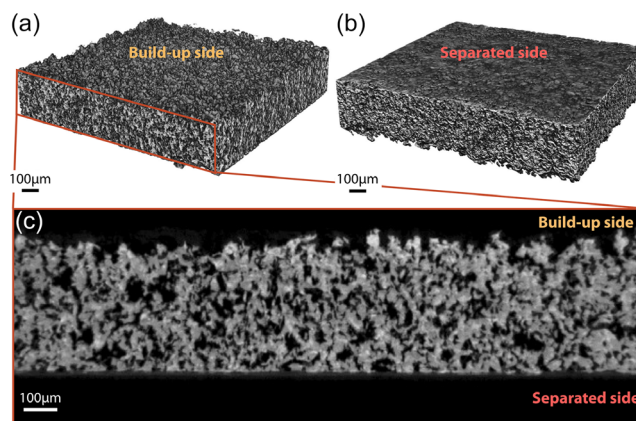

Figure 2. a,b) 3D reconstruction from X-ray microscopy (XRM) of thermally-sprayed PTL with a) buildup side on top and b) separated side on top. c) Virtual cross section through the PTL from XRM, displaying a rough buildup side (top) and a smooth separated side (bottom). Overview scan with 1.2 μm voxel size.

**ADVANCED
SCIENCE NEWS**

www.advancedsciencenews.com

**ADVANCED
ENGINEERING
MATERIALS**

www.aem-journal.com

Table 1. Comparison of average specific electrical resistance of the PTLs as sprayed and after heat treatment.

Specific electrical resistance in μΩ [m]	
As sprayed	Heat-treated
14.5 ± 0.3	9.5 ± 0.7

where a flat surface with decreased porosity is needed to maintain uninterrupted contact between catalyst and membrane.[39]

2.1.1. Effect of Heat Treatment

After removal from the substrate, the PTLs were heattreated in a vacuum at 700 °C for 15 min at 10^{-5} mbar intending to improve the electrical conductivity. The specific electrical resistance was measured by the 4-wire method. The results shown in **Table 1** indicate that the heat treatment increases the electrical conductivity by almost 35% compared to the as-sprayed PTLs. A possible explanation is a particle merging at increased temperature.

At the same time, the structural features should be preserved during heat treatment. The heat-treatment temperature and duration were selected to be significantly lower and shorter compared to the sintering of titanium powders for PTLs.[40] The aim was to avoid effects on the pore structure of the sprayed PTL. To verify that, SEM surface and cross-section images were taken. The SEM surface images of the buildup side and the separated side of a PTL as sprayed and after heat treatment are displayed in **Figure 3**a–f. The buildup side exhibits a similar morphology as sprayed and after heat treatment as shown in Figure 3a,d.
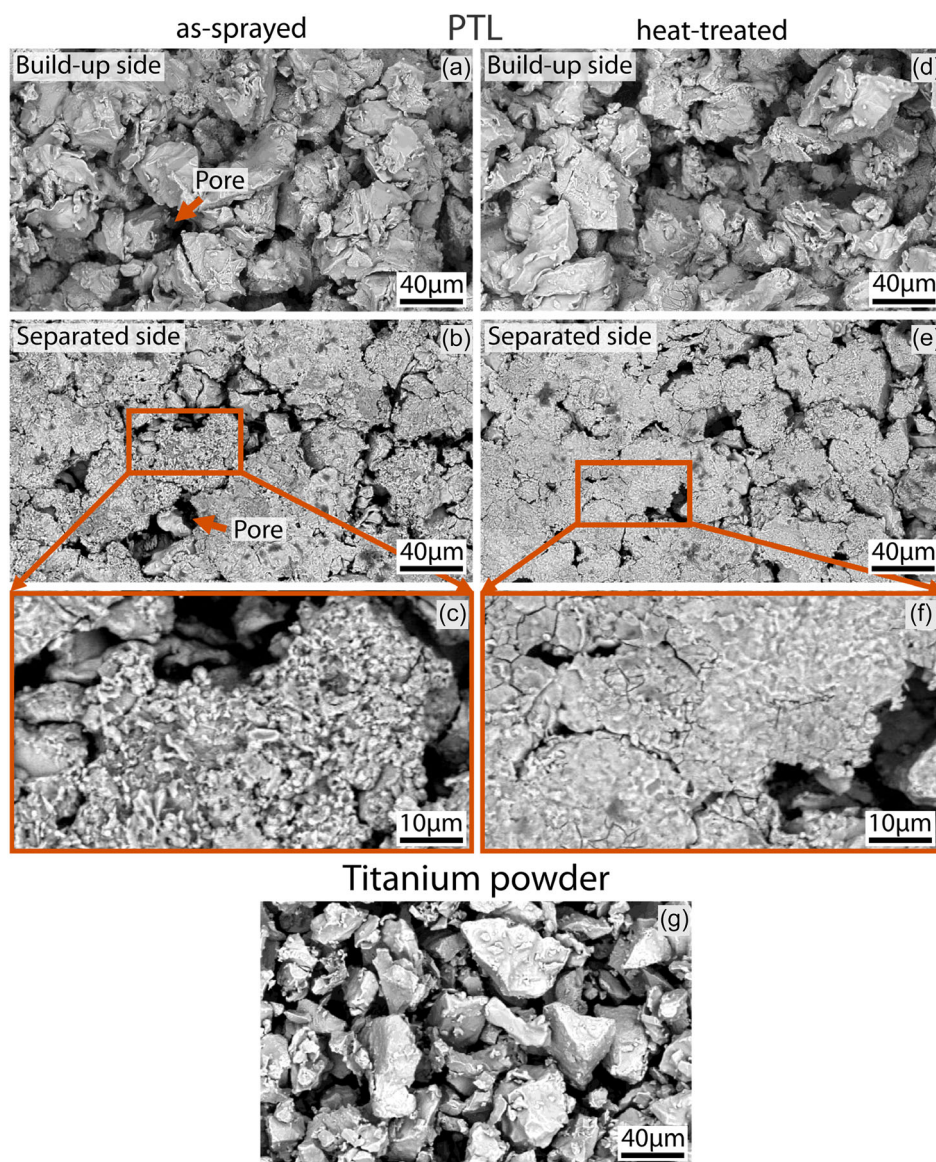

Figure 3. SEM surface images of a,d) the buildup side and b,c,e,f) the separated side of the PTLs. (a–c) The surface as sprayed and (d–f) the heat-treated surface. g) Titanium powder feedstock for HVOF process (grade 4, $F = -45 + 11 \mu m$).

Comparing the surface morphology on the separated side (Figure 3b,e) reveals a surface change after heat treatment. The surface appears smoother, and fine boundaries between titanium particles have been closed, as shown in the magnified images in Figure 3c,f. A merging of boundaries after heat treatment becomes additionally evident from the cross sections of the PTLs in **Figure 4** (compare Figure 4a,b with c,d). We attribute this to a sintering of the material and assume that the metallurgical bonding among particles is increased due to diffusion during heat treatment. An image analysis of the separated side of the PTL before and after heat treatment shows only a slight change in pore area, as depicted in Figure S1, Supporting Information. We conclude that the structural changes are insignificant compared to the improvement in electrical conductivity. Consequently, only heat-treated PTLs were used in the single-cell tests.

2.2. Structural Analysis of Feedstock Powder and PTLs

2.2.1. Morphology

To understand the formation of PTLs, the powder used for fabrication and the obtained PTLs are examined structurally. Figure 3g shows an SEM image of the titanium powder used. The irregular morphology of the powder particles stems from the production pathway by grinding hydrogenated titanium

and subsequently dehydrogenating the titanium hydride powder.[41]

Figure 3a shows that the buildup side of the obtained PTL mainly consists of titanium particles with very similar irregular morphology to those of the titanium powder in Figure 3g. Due to the inlet of hydrogen into the hot gas stream of the spraying process and thus the reduced combustion temperature, the titanium particles were molten slightly, maintaining their morphologies. Thus, the buildup side shows numerous pores and is rough. The average roughness Ra determined by CLSM is summarized in **Figure 5**a. Ra is much higher for the buildup side than for the substrate. In contrast, the separated side of the PTL exhibits a smooth surface with fewer pores (Figure 3b). It possesses a roughness similar to the substrate's roughness and is much smoother than the buildup surface. An explanation for this is that the impact of the underlying substrate and the additional application of titanium particles causes the first layers of titanium particles that were applied onto the substrate to deform more plastically than the titanium particles forming the interior coating. Thus, the particles on the surface of the buildup side appear undeformed.

The PTL cross sections in Figure 4a confirm that the titanium particles are slightly molten since the PTL consists of titanium particles instead of titanium lamellae, which form from molten titanium. Thus, we assume that mechanical interlocking is the
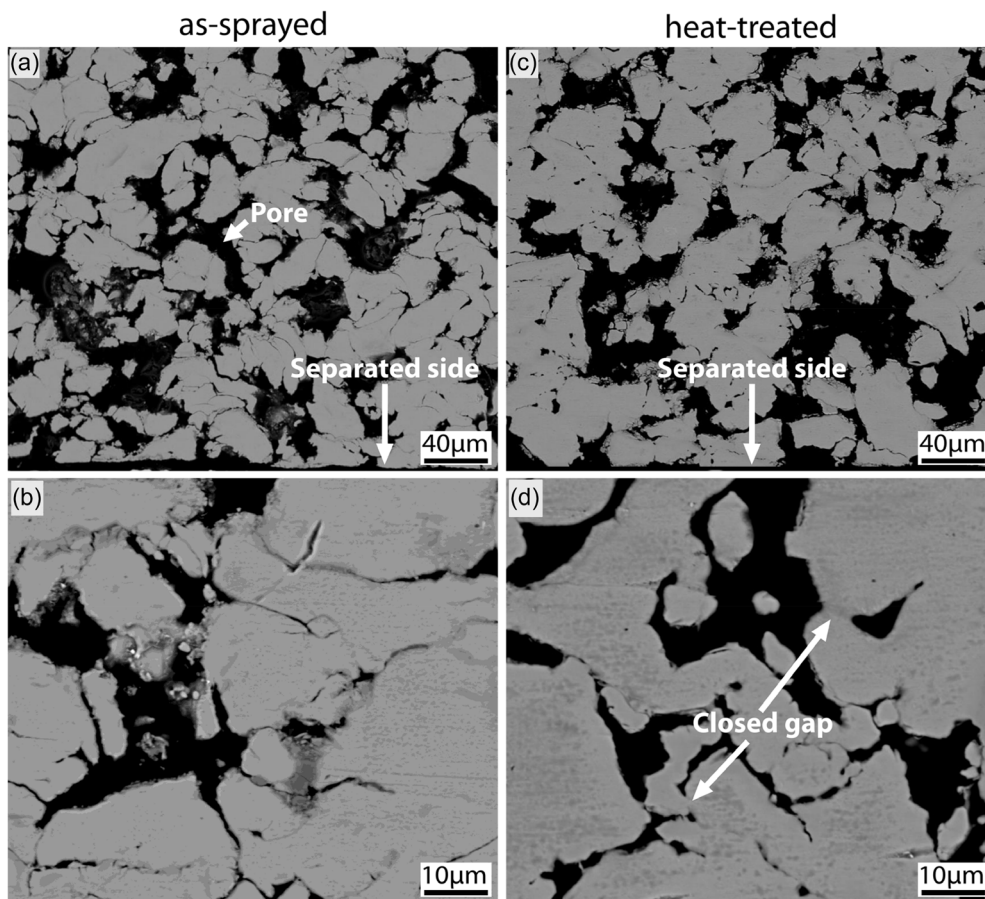

Figure 4. SEM images of the cross sections of the PTLs: a,b) as sprayed and c,d) after heat treatment.
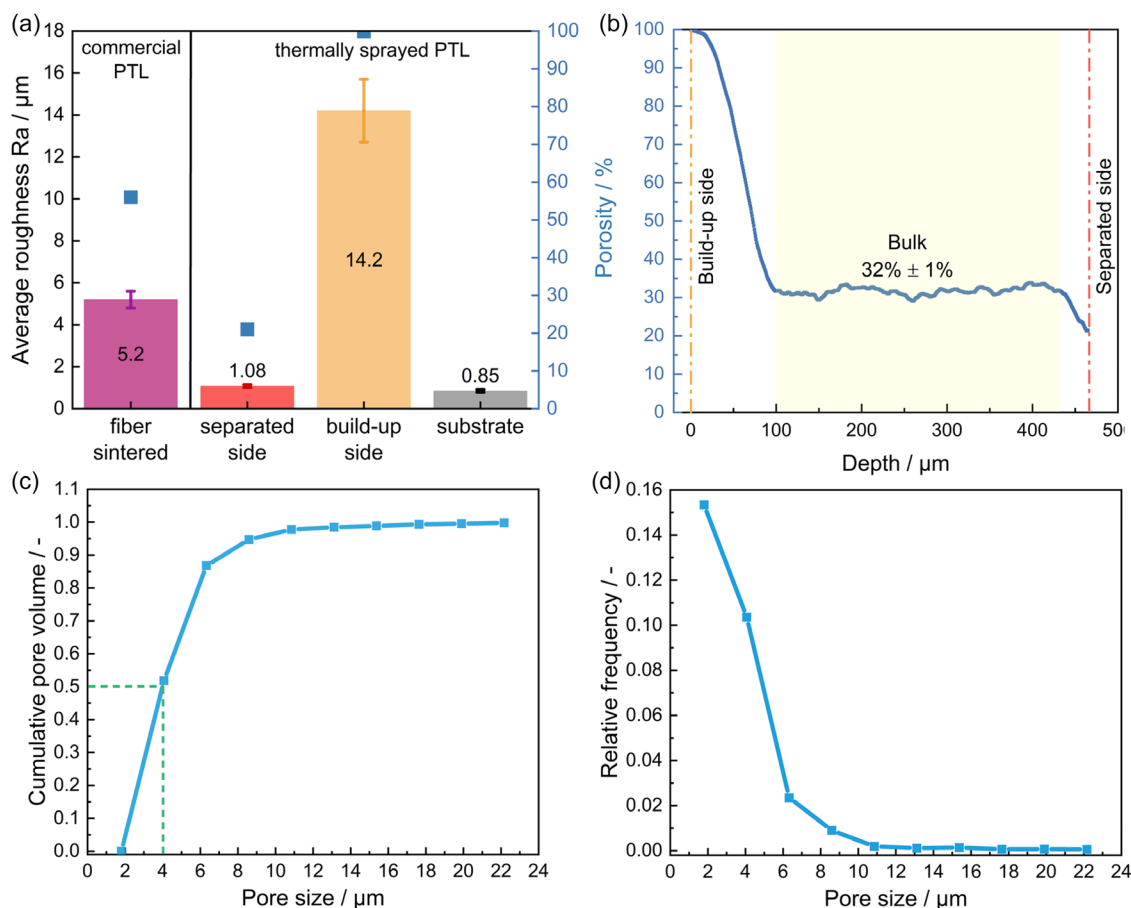
Figure 5. a) Average roughness Ra (bar plots) and porosity (blue squares) summarized for commercial and thermally-sprayed PTL. The bar plots show mean values including standard deviation. b) Porosity profile throughout the thickness of the thermally -sprayed PTL determined by XRM. Yellow-shaded range is used for averaging the bulk porosity. Dash-dotted lines mark the buildup and separated side. Note that the term porosity is also used here for the interface of the PTL. c,d) Pore size of thermally-sprayed PTL as (c) cumulative pore volume and (d) probability density function of pore size. The green-dashed line marks median pore size.

primary mechanism for the cohesion of the particles within the PTL before heat treatment.[31] As described earlier, the particles merge further by sintering during heat treatment.

2.2.2. Oxygen Content of PTLs

Since layers with low oxygen content are aimed for, we determined the oxygen content in the feedstock powder and the PTLs by carrier gas hot extraction, showing an oxygen mass content of 0.37 wt% for the feedstock titanium powder and 1.19 wt% for the as-sprayed PTL. In comparison, the commercial reference used in this work (Ti-fiber PTL from Bekaert) shows an oxygen content of 0.29 wt%. The increased oxygen content after spraying could relate to the fact that smaller titanium particles melt preferably during spraying due to their larger surface-to-volume ratio and lower heat capacities, causing them to swirl in-flight and to oxidize stronger.[31] In contrast, the oxidation of very slightly molten titanium particles is assumed to occur preferably on their surfaces because the diffusion of oxygen ions mainly controls the growth of oxides on particle surfaces.[31] Due to the very short

in-flight time of titanium particles as they are accelerated up to supersonic speed, and thus the very short diffusion time, oxidation is generally expected to be small.

2.2.3. Porosity and Pore Size of PTLs

The porosity of the as-sprayed PTLs is determined via SEM of PTL cross sections and for the heat-treated PTLs from XRM. Image analysis from SEM cross sections of the as-sprayed PTL yielded a mean porosity of 28% ± 3% throughout the entire volume. After heat treatment, the porosity did not change significantly, which is explained by the moderate temperature and relatively short duration of the heat treatment.

The thermally-sprayed PTL features an asymmetric structure, which is presumably beneficial for PEMWE operation, as discussed later. The XRM measurement gives insight into the porosity profile throughout the thickness of the PTL (Figure 5b). Based on this measurement, we partition the PTL into three parts: a layer on the buildup side, the bulk area, and a layer on the separated side. As mentioned before, the

buildup side has a high roughness; therefore, a porosity value for the surface is not easy to determine. The porosity in the layer close to the buildup side decreases within 100 µm until a mean porosity of 32% ± 1% in the bulk area is reached. Toward the separated side, the porosity drops to 21%. The higher porosity on the buildup side supports our hypothesis of coating densification by impacting particles during fabrication. The measured porosity can be considered very high for the HVOF process since HVOF-sprayed metallic coatings typically exhibit porosities of less than 1%.[32] We assume that the high porosity is due to the limited plastic deformation of the titanium particles during spraying which was sufficient for most titanium particles to adhere to the substrate but did not densify the coating too much while impacting. Due to this manufacturing feature, the unique porosity-zoned structure of the PTL is produced.

Figure 5c,d shows the pore size distribution, determined from XRM measurement, as cumulative pore volume and probability density function, respectively. Figure 5d shows that mainly pores below ≈6 µm are present in the PTL with a median pore size of ≈4 µm (Figure 5c). Note that most of the pores are close to the resolution limit with a voxel size of 670 nm. This pore size is small compared to commercially available materials, with a mean pore size of about 30 µm.[17,23,39] We elaborate on a possible influence on single-cell performance in Section 2.3.2.

2.3. Performance of PTLs in PEMWE Single-Cells

Thermally-sprayed PTLs were implemented in PEMWE single cells and tested for their performance in an electrochemical system. A commercially available Ti-fiber PTL (Bekaert, 56% porosity) was tested with the same parameters for comparison. The obtained polarization curves, the high-frequency resistance (HFR), and HFR-free polarization curves of both PTLs are displayed in **Figure 6**a,b. As can be seen from the polarization curves, the performance of the thermally-sprayed PTL is as good as the commercial PTL with 1.7 V at 2 A cm^{-2}. Also, the HFR of the two PTL types is with about 65 mΩ cm^2 similar. However, since the PTLs possess very different structures, this result will be analyzed based on possible influences.

2.3.1. Influence of PTL Bulk Properties

The measured HFR comprises the protonic resistance of the membrane, as well as the electrical bulk and contact resistances of the CL, PTL, and flow fields. The bulk resistance of the gold-coated Ti flow fields is assumed to be negligible, and the same type of commercial membrane was used in all measurements. Thus, changes in the HFR between the two PTLs stem from the electrical bulk resistance of the PTL or contact resistances of the PTL with flow field and CL.
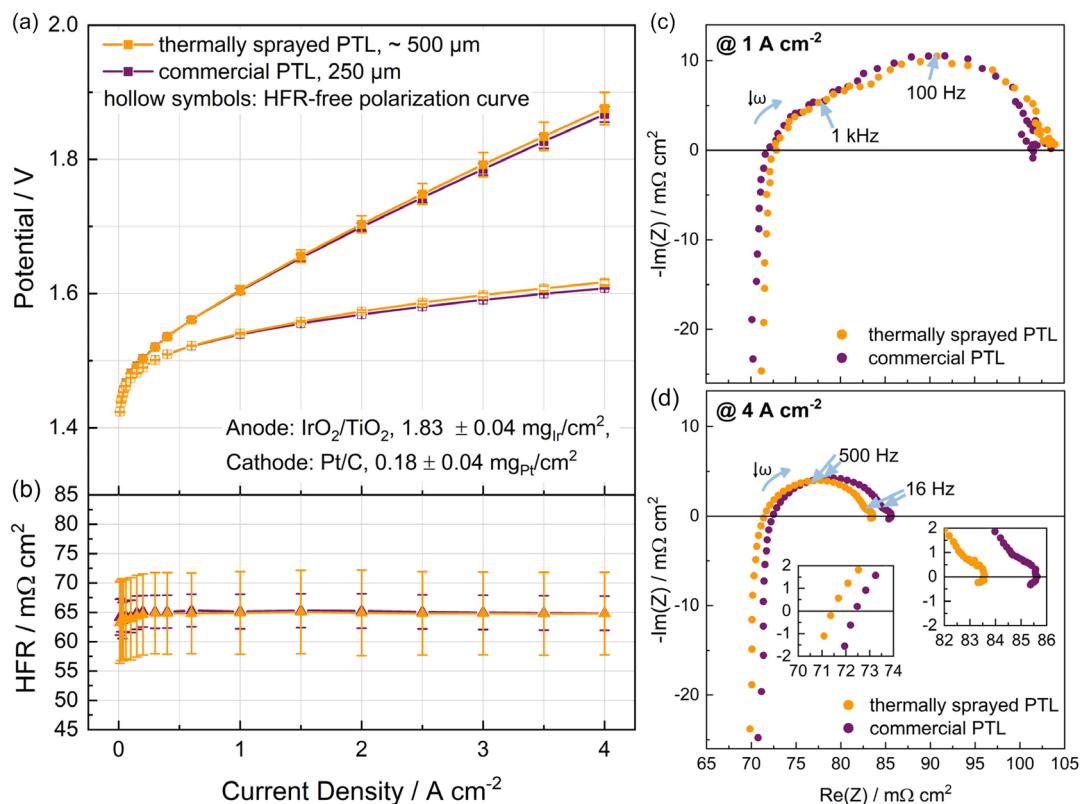

Figure 6. a) Polarization curves and b) high-frequency resistance (HFR) from electrochemical impedance spectroscopy (EIS) measurement. c,d) Nyquist plots from EIS measurement at c) 1 A cm^{-2} and d) 4 A cm^{-2}. A Nafion 212 membrane (≈51 µm) and a compression of 24.7 ± 1.6% were used for all tests. All measurements were repeated three times with pristine components, and the standard deviation is given for the polarization curves.

Starting with the electrical bulk resistance, the thickness difference between thermally-sprayed and commercial PTL must be considered. Even though the PTLs differ twofold in thickness (thermally sprayed 500 µm vs commercial 250 µm), they have HFR values of about 65 mΩ cm^2 (Figure 6b). Previous publications showed contradicting trends regarding thickness variations: Improved performance with thinner[20,42,43] or decreased performance with thinner PTLs.[23,44] However, these publications compare PTLs of different structures, making a direct comparison challenging. Nevertheless, heat-transfer resistance was shown to increase the HFR with increasing PTL thickness.[23,45] In our case, however, a high water flow might overshadow such an effect.

Since a difference between the samples in our measurement is not visible, we hypothesize that the influence of the thickness is smaller than the influence of the surface properties, which will be discussed in Section 2.3.2. Consequently, a higher thickness of the PTL does not seem to be detrimental concerning Ohmic resistance for the two materials compared in this study.

Based on the ex situ electrical resistance and single-cell measurements, we exclude an increased electrical bulk resistance that would be caused by a thick oxide layer on the Ti particles built during thermal spraying under non-inert conditions that would obstruct the electrical pathway throughout the PTL. This result is supported by the low oxygen content of 1.19 wt% in the as-sprayed PTLs (Section 2.2.2).

The HFR-free polarization curves in Figure 6a overlap up to a current density of 2 A cm^{-2}. For higher current densities, the HFR-free polarization curve of the tests with thermally-sprayed PTL shows a slightly higher cell potential of 4–9 mV than that of commercial PTLs. This deviation could indicate that mass transport is a limiting factor, although this interpretation must be treated carefully, as the deviations are small.

In general, the thermally-sprayed PTL possesses a lower mean porosity (32% ± 1%) and smaller pores (4 µm median pore size) than the commercial PTL having a mean porosity of 56% and mean pore size of 30 µm[39] (cf. Figure 5). A difference in tortuosity between the two PTLs could further lead to a difference in mass transport.[46] Judging from the structure, it could be possible that produced oxygen is transported out slower or is more likely to get stuck in our fabricated PTLs.[15] In contrast, a hierarchically structured porosity was shown to be beneficial in terms of oxygen removal when the porosity increases from CL to flow field.[47] To assess the mass transport, the Nyquist plots at low and high current densities can be compared. Figure 6c,d shows similar Nyquist plots of the two different PTLs at both current densities. An additional semicircle forming in the low-frequency region at higher current densities is visible for both PTLs at the same frequency of about 16 Hz. The formation of a semicircle at higher current densities is often attributed to diffusion losses, which include mass transport hindrance due to two-phase flow.[19,25] Since this phenomenon is observed for both PTL materials to the same extent and their overall performance is state of the art, a mass transport issue is considered minor at our cell dimension.

2.3.2. Influence of PTL Surface Properties

The difference in surface morphology between the two tested PTLs must be considered because of its possible influence on interfacial contact resistance (ICR), catalyst utilization, and mass transport. The difference stems not only from the fabrication method used but also from the type of feedstock material: titanium powder for the sprayed PTLs or fibers for the commercial PTL. The morphological properties examined are surface roughness, porosity, and pore size. As shown in Figure 5a, the separated side of the thermally-sprayed PTLs possesses a smaller roughness Ra compared to the commercial PTL (thermally sprayed, separated side: Ra = 1.08 ± 0.07 µm vs commercial: Ra = 5.2 ± 0.4 µm). The buildup side, in contrast, has a higher roughness than the commercial PTL (thermally sprayed, buildup side: Ra = 14.2 ± 1.5 µm vs commercial: Ra = 5.2 ± 0.4 µm).

The difference in surface roughness on the two sides of the thermally-sprayed PTL also becomes evident from the XRM 3D reconstruction in Figure 2a,b. Judging from the roughness, two effects are possible: on the one hand, a smaller roughness leads to a lower interfacial contact area toward the CL because the membrane with CL can bend around the particles/fibers. Consequently, the contact area would depend on the deformation of the membrane.[22] On the other hand, lower roughness prevents a deformation of the CL as shown in the SEM images in Figure S2, Supporting Information. In Figure S2, Supporting Information, it is clearly visible that a high deformation caused by a PTL with higher roughness is not visible when using the thermally-sprayed PTL. This is especially relevant for low-loading CLs where it was shown that a lower roughness prevents CL cracking and, consequently, disconnection.[48,49] Conversely, the higher roughness of the thermally-sprayed PTLs facing the flow fields could lead to a lower contact area, increasing the contact resistance since the flow fields do not intrude into the PTL valleys.

Another important parameter influencing the ICR is the porosity that determines the contact area.[48,49] It was shown that decreasing the porosity facing the CL (either as bulk porosity or via an additional layer) decreased the HFR.[20,26] The porosity facing the CL of the thermally-sprayed PTL is decreased by roughly 35% compared to the commercial PTL (thermally sprayed, separated side ≈21% vs commercial ≈56%). However, despite these morphology differences, the tested PTLs show similar HFRs (Figure 6b). A possible explanation is that an increasing loss, such as an increased contact resistance between PTL and flow field, compensates for the different interface qualities. It is also possible that the highly conductive CL used, mitigates any contact improvements.[27] This would render the interface less critical because the CL can conduct electrons to places without direct contact with the PTL, i.e., the pore area, and, therefore, compensate for suboptimal surface properties.[27,50]

To check if the structural change of the interface PTL–CL introduces additional effects in the kinetic region, a Tafel analysis is shown in Figure S3, Supporting Information. Tafel slopes are derived as the slope of the HFR-free polarization curves in a low-current-density region where Ohmic overpotentials, mass transport overpotentials, and impact from the cathode side are assumed to be negligible. The Tafel slopes for the cell tests with thermally-sprayed and commercial PTL do not show a significant difference with 50.5 ± 0.3 and 50.9 ± 0.2 mV dec^{-1}, respectively. The values agree with literature values ranging between 45 and 50 mV dec^{-1} for the same catalyst material at similar loadings.[51]

We conclude that the catalyst contacting is not negatively influenced by the different surface morphology of the thermally-sprayed PTL. However, it is also not visible from the data that the lower porosity and the related higher volume fraction of PTL material contacting the CL are beneficial. Similar to the influence on Ohmic resistances, such an effect may only be visible in lower Ir-loading tests where the CL tends to become discontinuous, and the PTL does not compensate for this effect due to its large pores.[50] An influence on the Tafel slope was shown in literature when comparing low and ultralow loading with surface-modified PTLs: only for the ultralow loading case did the difference become visible in the Tafel slope.[21] A difference could become apparent for lower loaded (i.e., thin and noncontiguous) CLs but also for catalyst material with lower conductivity or a catalyst-coated substrate approach (e.g., a PTE). While for a lower-loaded or less conductive CL, porosity and pore size are more relevant due to interfacial contact area,[21] for a PTE, the roughness in combination with pore size is crucial to assure the ionic connection of the catalyst material.[39]

Even though the performances of thermally-sprayed and commercial PTL are similar, the thermally-sprayed PTL shows a larger error bar. Since this is very pronounced for the HFR, the deviation over the repeated measurements possibly originates from the contact resistance of the PTL–CL or BPP–PTL interface. A possible explanation is based on the mechanical pressure on the active area in the cell. It is calculated based on the mean PTL thickness. However, the thickness of the different PTL samples throughout the batches and over the 5 cm^2 area varied; thus, we hypothesize that differences in compression could lead to a variation in ICR, causing larger measurement deviations.

Lastly, the thermally-sprayed PTL was tested for degradation stability in a single cell for 160 h as shown in Figure S4, Supporting Information. The degradation rate slows down after roughly 15 h of testing to 0.171 ± 0.001 mV h^{-1} over the remaining 145 h. We assume a large part of the degradation originating from a buildup of contact resistance due to titanium surface oxidation.[52] Under constant current and reaction conditions (i.e., temperature, pressure, reactant flow), it has been observed that the growth of the passivation layer slows down after reaching a certain thickness due to oxygen-diffusion limited growth, as the surface becomes passivated against dissolution.[9,53] This phenomenon may explain the observed reduction in the degradation rate after 15 h, potentially attributable to the slowing down of the oxidation layer formation. The degradation rate in this study is higher compared to similar testing of the commercial PTL in our previous work.[6] However, in this case, a platinum coating was used. It was shown that a protective coating can minimize a resistance increase due to passivation.[52] Thus, we assume that a passivation of the titanium causing contact resistance is contributing to this higher degradation rate. Deconvolution of the degradation mechanisms, however, requires further investigation which is beyond the scope of this work but should be utilized to further improve the performance of the thermally-sprayed PTL in PEMWE.

In this study, two PTLs of very different morphology were compared: a thermally-sprayed PTL with different zones of porosity (mean porosity ≈32%) and a median pore size of about 4 μm versus a commercial fiber-sintered PTL with 56% porosity and a pore size ≈30 μm.[17,23,39] Nevertheless, we showed that competitive performance in PEMWE single cells is possible with thermally-sprayed PTLs via HVOF spraying.

Importantly, HVOF spraying promises several advantages on the fabrication level, e.g., lower costs than VPS, high suitability for scale-up, and simplified, chemical-free removal of the PTL from the substrate. Due to their reduced roughness and pore size, a further application of the thermally-sprayed PTLs as PTEs is highly interesting. Our PTL structure is beneficial in preventing catalyst particles from penetrating PTL pores and, thus, from being ionically disconnected.[2,39] Hence, this structure shows promising features for PTE design, which will be investigated in our future work.

3. Conclusion

This study presents porosity-zoned PTLs for PEMWE prepared from titanium powder using HVOF spraying. The PTLs were investigated in terms of surface topography and bulk structure, and the performance in PEMWE single-cell tests was compared to commercial PTL material.

The important findings are summarized as follows. 1) The PTLs feature two sides of different porosity and roughness. The roughness, porosity, and pore size facing the CL are decreased compared to those of the commercial material. The mean bulk porosity equals 32% ± 1%. 2) When implemented in PEMWE single cells, the PTLs show highly similar performances compared to commercially available materials, emphasizing their suitability for this technology. 3) The PTLs have a low oxygen content for a thermally-sprayed product of 1.19 wt%. 4) The substrates used for HVOF spraying ensured a highly reproducible mechanical coating separation. 5) The heat treatment improved the electrical conductivity of the PTLs but did not alter their porosity and pore size distribution.

With the presented approach for PTL manufacturing, several advantages compared to VPS stand out: lower costs and simplified mechanical removal of the PTL from the spray substrate. Additionally, the microporous structure on the separated side is possibly beneficial in improving the interface toward the CL, and a competitive performance when used in PEMWE single cells is possible. This provides several opportunities for PEMWE design optimization and cost reduction.

4. Experimental Section

PTLs were fabricated by thermal spraying followed by a heat-treatment step as described in the following.

Thermal Spraying: A DJ2600 HVOF spray system (Oerlikon Metco, Pfäffikon, Switzerland) was used for the coating application. The system used hydrogen as fuel gas and nitrogen as shielding and carrier gas. Free-standing PTLs were obtained by applying titanium coatings onto a substrate and subsequently separating the PTLs from the substrate. The spray parameters listed in **Table 2** were used in the spray process and were identified as the most suitable by the preceding process development shown in our previous work.[37] Substrates with a size of L × W × H = 50 × 50 × 5 mm^3 and a low average roughness Ra < 1 μm were used in the spraying process. The substrates were cleaned with ethanol before the coating process. The PTLs were separated mechanically from the substrate with the aid of a piece of paper (cf. Figure 1b,c). As powder feedstock in the HVOF process, a titanium powder, grade 4, with

Table 2. Spray parameters used for PTL fabrication on the DJ2600 HVOF spray system.

H$_2$ in SLPM[a]	O$_2$ in SLPM	N$_2$ in SLPM	Distance [mm]	Robot velocity [mm s^{-1}]	Meander width [mm]
340–440	45–65	300–350	150–200	1500	3.6

[a]Standard liter per minute.

a particle size distribution of $f = -45 + 11\,\mu m$ (Oerlikon Metco Europe GmbH, Raunheim, Germany) was used.

Heat Treatment: Ten separated PTLs were heat-treated in a vacuum furnace (PVA MOV 553 T, PVA TePla AG). The heat treatment was carried out at 700 °C for 15 min at 10^{-5} mbar. Only heat-treated PTLs were used in the PEMWE single-cell tests due to their higher electrical conductivity compared to the PTLs as sprayed.

4-Wire (Kelvin) Measurement: The 4-wire method was used to determine the specific electrical resistance of the PTLs before and after heat treatment. The milliohm meter ILOM 508 A by ISO-TECH with two clamps was attached to the sample. Each clamp consisted of two contacts isolated against each other, allowing the application of a test current and a voltage drop measurement.

A physical characterization of the used powder, used substrate, and obtained PTLs was conducted with the following techniques.

SEM: An SEM (Phenom XL, Thermo Fisher Scientific) at an acceleration voltage of 15 kV was used to examine the surface morphology of the titanium powder as well as the surface of the PTLs as sprayed and after heat treatment. For the cross-section analysis, the PTLs were cut by a scissor and embedded with epoxy resin. To obtain cross sections, the embedded PTLs were grinded until #2400 SiC paper and consecutively polished with diamond suspension until a grain size of 1 μm. To determine the porosity of the PTL surfaces, image analysis of micrographs was carried out using ImageJ.[54] Ten SEM images of a PTL were used for an average value.

Carrier Gas Hot Extraction: The oxygen mass content of the titanium powder and the as-sprayed PTLs was analyzed using carrier gas hot extraction by Eltra Elementrac ONH-p at IME Process Metallurgy and Metal Recycling, RWTH Aachen University.

CLSM: To determine the average roughness Ra of the substrate and the separated PTLs, a CLSM (VK-X210, Keyence Deutschland GmbH) was used.

XRM: XRM was used to determine the porosity and pore size distribution of the obtained PTLs. It was performed with a Zeiss Xradia Versa 620 (Carl Zeiss X-ray Microscopy Inc., Pleasanton, CA, USA), equipped with a high-framerate CMOS detector. A total of 1601 X-ray projections were recorded at different angles and reconstructed by proprietary software (Zeiss XMReconstructor, Carl Zeiss Xray Microscopy Inc., Pleasanton, CA, USA) with a filtered back-projection algorithm. The resulting volumetric images had a 3D isotropic voxel size of 1.2 μm (overview scan) and 670 nm (detail scan). The high resolution was achieved by combining geometric magnification from the cone-shaped X-ray beam with geometrical magnification with a 4x (overview) and 20x (detail) objective, respectively. The 1.2 μm voxel size scan was recorded with 0.8 s exposure time and a framerate of 44 with a voltage of 40 kV and 3 W power. For the 670 nm scan, an exposure of 0.9 s with 12 frames per second and binning 2 were implemented with a voltage of 80 kV and 10 W power.

XRM data visualization and quantification were performed with the workflow-based modular software XamFlow (Lucid Concepts AG, Zürich, Switzerland). Binary images were created by grey value thresholding and served as a basis for the porosity calculation. A Python script, utilizing the scikit-image library,[55] was used to compute porosity metrics by iteratively analyzing connected components in each image slice along the z axis while filtering out objects with an area below 15 pixels.

For the determination of the pore size distribution, binarization with a threshold of 140 was followed by the calculation of slice-wise porosity in

x, y, and z directions using PoreSpy.[56] Local thickness-based pore size distribution (psd) was extracted to minimize artifacts, and both the cumulative density function (cdf) and probability density function (pdf) were computed.

Catalyst-Coated Membrane Fabrication: Catalyst-coated membranes (CCMs) were manufactured via the decal transfer technique where 5 cm^2 sized electrodes coated onto a substrate are united with a ≈51 μm thick Nafion NR212 membrane (Chemours, USA) by a hot-pressing step at $T = 155$ °C and $p = 2.5$ MPa. The loadings of the electrodes were determined by weighing the decals before and after hot pressing.

The catalyst inks were prepared from a mixture of the respective catalyst powder with suitable solvents and ionomer dispersion. For the anode, IrO$_2$/TiO$_2$ catalyst powder (Elyst Ir75 0480 from Umicore) was mixed with deionized (DI) water, 1-propanol (>99.5% from Sigma-Aldrich, USA), and ionomer dispersion Nafion D2021 (Chemours, USA) with a water content of 10 wt%, an ionomer to catalyst ratio of 13.12 wt%, and a total solid content of 0.46 g ml$_{ink}^{-1}$. On the cathode, platinum supported on carbon catalyst powder (Pt/C, TEC10V40E from Tanaka, Japan) was mixed with DI water, 1-propanol, and Nafion D2021 ionomer dispersion with a water content of 10 wt%, an ionomer to carbon ratio of 28 wt%, and a total solid content of 0.05 g ml$_{ink}^{-1}$. The inks were suspended for 24 h using a roller mixer (BTR5-12 V from Ratek, Australia) with zirconium beads ($\varnothing = 5$ mm from Fritsch GmbH) at 180 and 60 rpm for anode and cathode inks, respectively. From the inks, electrodes were coated onto 50 μm thick PTFE substrates (Angst + Pfister) utilizing the Mayer rod technique (rods from ERICHSEN GmbH & Co. KG). The electrode sheets were dried for 2 h at 70 °C (furnace ED56 from BINDER, Germany) before being cut into 5 cm^2 electrodes and hot pressed with membranes.

Single-Cell Tests of PTLs in PEMWE Setup: All single-cell tests were performed on a commercial test bench (600 Electrolyzer Test System, Scribner LLC) equipped with a potentiostat with a current booster (BioLogic VSP-300). An in-house designed cell fixture adapted from previous works[51] with an active area of 5 cm^2 was used. For the cell assembly, a CCM was sandwiched between PTL and flow fields inside the cell. As PTL on the anode side, either a thermally-sprayed PTL or a commercial Ti-fiber PTL (2GDL10-0,25 from NV Bekaert SA, Belgium) was used. Since the thermally-sprayed PTLs feature two sides with different surface roughness and porosity, the smoother side was oriented toward the CCM. A carbon PTL with a microporous layer (H24C5 Freudenberg & Co. KG) was used on the cathode. For all tests, CCMs with loadings of 1.83 ± 0.04 mg$_{Ir}$ cm^{-2} (IrO$_2$/TiO$_2$ Elyst Ir75 0480, Umicore) on the anode and 0.18 ± 0.04 mg$_{Pt}$ cm^{-2} (Pt/C, TEC10V40E, Tanaka) on the cathode were used. Gasket thicknesses were chosen to compress the carbon PTL by $24.7\% \pm 1.6\%$.

The anode was flushed with 100 mL min^{-1} DI water (18.2 MΩ cm) which was additionally purged with nitrogen for 10 min prior to testing to remove dissolved CO$_2$ from refilling of the tank. The anode feed was heated throughout the test to 80 °C. The cathode was kept dry, and the venting line was purged with nitrogen for safety reasons. The cell was kept at 80 °C during the testing time with cartridge heaters placed into both endplates and regulated by a thermocouple placed into the cathodic flow field plate. Once the cell temperature and anode feed reached 80 °C, a 30 min period was given for equilibration before the test was started. The first steps of the test were an electrical short test at 1 V for 1 min followed by a conditioning step of 30 min at 1 A cm^{-2}. Afterward, three subsequent polarization curves were acquired between 0.01 and 4 A cm^{-2}, holding each current density step for 5 min to ensure steady-state conditions and averaging the last 30 data points (=15 s) for analysis.

Galvanostatic electrochemical impedance spectroscopy (EIS) was measured in a frequency range from 100 kHz to 500 mHz at each point of the polarization curve after the respective current density hold. To ensure a good signal-to-noise ratio and a linear system response, the perturbation of each alternating current (AC) was chosen to be ≤10% of the AC but not smaller than 20 mA. Since the first two polarization curves were considered part of conditioning, it was checked every time if the last two polarization curves overlap and only the last polarization curve was taken for analysis. All tests were repeated three times for reproducibility.

Data Evaluation for Single-Cell Tests: HFR values were extracted from EIS measurements as described in previous work.[6] In short, each current density was fitted in a frequency range of 50–0.5 kHz with an equivalent circuit model comprising an inductance, a resistor, and a transmission line model in series.[57,58] An adjusted coefficient of determination ($R^2_{adj} \geq 0.99$) was used. R^2_{adj} was calculated separately for the real and imaginary parts and was subsequently averaged to yield a fit quality indicator for the fit. Fitting was performed using an in-house developed Python routine based on NumPy,[59] SciPy,[60] pandas,[61,62] matplotlib,[63] and impedance.py.[64] HFR-free polarization curves were derived by subtracting the product of HFR and the corresponding current density from the polarization curve. For the Tafel analysis, the lower-current-density region of the HFR-free polarization curves was plotted in a semilogarithmic plot. In a current density range between 0.01 and 0.1 A cm^{-2}, influences from Ohmic and mass transport resistances were assumed to be negligible and cathode kinetics were assumed to be much faster than anode kinetics. Thus, Tafel slopes were derived from a logarithmic fit in this current-density range.

Supporting Information

Supporting Information is available from the Wiley Online Library or from the author.

Conflict of Interest

The authors declare no conflict of interest.

Author Contributions

Kirsten Bobzin and Selina Finger contributed equally to this work. **Kirsten Bobzin**: funding acquisition (equal); project administration (equal); resources (equal); supervision (equal); and writing—review and editing (equal). **Selina Finger**: conceptualization (equal); data curation (equal); formal analysis (equal); investigation (equal); methodology (equal); software (equal); validation (equal); visualization (equal); writing—original draft (equal); and writing—review and editing (equal). **Lidong Zhao**: conceptualization (equal); methodology (equal); writing—original draft (equal); and writing—review and editing (equal). **Hendrik Heinemann**: writing—review and editing (supporting). **Elisa Olesch**: writing—review and editing (supporting). **Katja Radermacher**: writing—review and editing (supporting). **Sabrina Pechmann**: formal analysis (supporting); investigation (supporting); writing—review and editing (supporting). **Dennis Possart**: formal analysis (supporting); investigation (supporting); and writing—review and editing (supporting); **Silke H. Christiansen**: resources (supporting) and writing—review and editing (supporting). **Darius Hoffmeister**: validation (supporting) and writing–review and editing (supporting). **Birk Fritsch**: data curation (supporting); methodology (supporting); software (equal); and writing—review and editing (equal). **Simon Thiele**: funding acquisition (equal); project administration (equal); resources (equal); supervision (equal); writing—review and editing (supporting). **Andreas Hutzler**: conceptualization (supporting); funding acquisition (equal); project administration (equal); resources (equal); supervision (equal); and writing—review and editing (equal).

[1] M. Bernt, A. Hartig-Weiß, M. F. Tovini, H. A. El-Sayed, C. Schramm, J. Schröter, C. Gebauer, H. A. Gasteiger, *Chem. Ing. Tech.* **2020**, *92*, 31.

[2] C. van Pham, D. Escalera-López, K. J. Mayrhofer, S. Cherevko, S. Thiele, *Adv. Energy Mater.* **2021**, *269*, 118762.

[3] A. Mayyas, M. Ruth, B. Pivovar, G. Bender, K. Wipke, *Manufacturing Cost Analysis for Proton Exchange Membrane Water Electrolyzers*. National Renewable Enery Laboratory. NREL/TP-6A20-72740.2. Golden, CO **2019**.

[4] M. Carmo, D. L. Fritz, J. Mergel, D. Stolten, *Int. J. Hydrog. Energy* **2013**, *38*, 4901.

[5] C. van Pham, M. Bühler, J. Knöppel, M. Bierling, D. Seeberger, D. Escalera-López, K. J. Mayrhofer, S. Cherevko, S. Thiele, *Appl. Catal. B: Environ.* **2020**, *269*, 118762.

[6] D. Hoffmeister, S. Finger, L. Fiedler, T.-C. Ma, A. Körner, M. Zlatar, B. Fritsch, K. W. Bodnar, S. Carl, A. Götz, B. A. Zubiri, J. Will, E. Spiecker, S. Cherevko, A. T. S. Freiberg, K. J. J. Mayrhofer, S. Thiele, A. Hutzler, C. van Pham, *Adv. Sci.* **2024**, *11*, e2402991.

[7] Y. N. Regmi, E. Tzanetopoulos, G. Zeng, X. Peng, D. I. Kushner, T. A. Kistler, L. A. King, N. Danilovic, *ACS Catal.* **2020**, *10*, 13125.

[8] P. Mazúr, J. Polonský, M. Paidar, K. Bouzek, *Int. J. Hydrogen Energy* **2012**, *37*, 12081.

[9] L. Fiedler, T.-C. Ma, B. Fritsch, J. H. Risse, M. Lechner, D. Dworschak, M. Merklein, K. J. J. Mayrhofer, A. Hutzler, *ChemElectroChem* **2023**, *10*, e202300373.

[10] H. Teuku, I. Alshami, J. Goh, M. S. Masdar, K. S. Loh, *Int. J. Energy Res.* **2021**, *45*, 20583.

[11] E. Taibi, H. Blanco, R. Miranda, M. Carmo, D. Gielen, R. Roesch, *Green Hydrogen Cost Reduction: Scaling Up Electrolysers to Meet the 1.5 °C Climate Goal*, International Renewable Energy Agency (IRENA), Abu Dhabi **2020**.

[12] M. Kroschel, A. Bonakdarpour, J. T. H. Kwan, P. Strasser, D. P. Wilkinson, *Electrochim. Acta* **2019**, *317*, 722.

[13] T. L. Doan, H. E. Lee, S. S. H. Shah, M. Kim, C.-H. Kim, H.-S. Cho, T. Kim, *Int. J. Energy Res.* **2021**, *45*, 14207.

[14] T. Schuler, J. M. Ciccone, B. Krentscher, F. Marone, C. Peter, T. J. Schmidt, F. N. Büchi, *Adv. Energy Mater.* **2020**, *10*, 1903216.

[15] X. Peng, P. Satjaritanun, Z. Taie, L. Wiles, A. Keane, C. Capuano, I. V. Zenyuk, N. Danilovic, *Adv. Sci.* **2021**, *8*, e2102950.

[16] R. Bock, H. Karoliussen, F. Seland, B. G. Pollet, M. S. Thomassen, S. Holdcroft, O. S. Burheim, *Int. J. Hydrog. Energy* **2020**, *45*, 1236.

[17] T. Schuler, C. C. Weber, J. A. Wrubel, L. Gubler, B. Pivovar, F. N. Büchi, G. Bender, *Adv. Energy Mater.* **2024**, *14*, 2302786.

[18] M. Bernt, A. Siebel, H. A. Gasteiger, *J. Electrochem. Soc.* **2018**, *165*, F305.

[19] Z. Kang, S. M. Alia, J. L. Young, G. Bender, *Electrochim. Acta* **2020**, *354*, 136641.

[20] Z. Kang, J. Mo, G. Yang, S. T. Retterer, D. A. Cullen, T. J. Toops, J. B. Green Jr, M. M. Mench, F.-Y. Zhang, *Energy Environ. Sci.* **2017**, *10*, 166.

[21] J. K. Lee, T. Schuler, G. Bender, M. Sabharwal, X. Peng, A. Z. Weber, N. Danilovic, *Appl. Energy* **2023**, *336*, 120853.

[22] T. Schuler, R. de Bruycker, T. J. Schmidt, F. N. Büchi, *J. Electrochem. Soc.* **2019**, *166*, F270.

[23] C. C. Weber, T. Schuler, R. de Bruycker, L. Gubler, F. N. Büchi, S. de Angelis, *J. Power Sources Adv.* **2022**, *15*, 100095.

[24] T.-C. Ma, A. Hutzler, B. Bensmann, R. Hanke-Rauschenbach, S. Thiele, *J. Electrochem. Soc.* **2024**, *171*, 44504.

[25] S. Stiber, H. Balzer, A. Wierhake, F. J. Wirkert, J. Roth, U. Rost, M. Brodmann, J. K. Lee, A. Bazylak, W. Waiblinger, A. S. Gago, K. A. Friedrich, *Adv. Energy Mater.* **2021**, *11*, 2100630.

[26] P. Lettenmeier, S. Kolb, F. Burggraf, A. S. Gago, K. A. Friedrich, *J. Power Sources* **2016**, *311*, 153.

[27] C. C. Weber, S. de Angelis, R. Meinert, C. Appel, M. Holler, M. Guizar-Sicairos, L. Gubler, F. N. Büchi, *EES Catal.* **2024**, *2*, 585.

[28] P. Lettenmeier, S. Kolb, N. Sata, A. Fallisch, L. Zielke, S. Thiele, A. S. Gago, K. A. Friedrich, *Energy Environ. Sci.* **2017**, *10*, 2521.

[29] K. E. Ayers, C. Capuano, E. B. Anderson, *ECS Trans.* **2012**, *41*, 15.

[30] M. Suermann, T. Gimpel, L. V. Bühre, W. Schade, B. Bensmann, R. Hanke-Rauschenbach, *J. Mater. Chem. A* **2020**, *8*, 4898.

[31] P. L. Fauchais, J. V. Heberlein, M. I. Boulos, *Thermal Spray Fundamentals*, Springer US, Boston, MA **2014**.

[32] J. R. Davis, *Handbook of Thermal Spray Technology*, ASM International, OH, USA **2004**.

[33] A. Geibel, L. Froyen, L. Delaey, K. U. Leuven, *J. Therm. Spray Technol.* **1996**, *5*, 419.

[34] M. Helali, M. Hashmi, *J. Mater. Process. Technol.* **1996**, *56*, 431.

[35] Y. Zhao, L. Wang, J. Yang, D. Li, X. Zhong, H. Zhao, F. Shao, S. Tao, *J. Therm. Spray Technol.* **2015**, *24*, 338.

[36] E. Lugscheider, C. Herbst, L. Zhao, *Surf. Coat. Technol.* **1998**, *108*, 16.

[37] K. Bobzin, L. Zhao, H. Heinemann, E. Olesch, in *Thermal Spray 2024: Proceedings from the Inter. Thermal Spray Conf.*, ASM International, OH, USA **2024**, p. 291.

[38] T. W. Clyne, S. C. Gill, *J. Therm. Spray Technol.* **1996**, *5*, 401.

[39] M. Bierling, D. McLaughlin, B. Mayerhöfer, S. Thiele, *Adv. Energy Mater.* **2023**, *13*, 2203636.

[40] J. K. Lee, G. Y. Lau, M. Sabharwal, A. Z. Weber, X. Peng, M. C. Tucker, *J. Power Sources* **2023**, *559*, 232606.

[41] F. H. Froes, *Titanium Powder Metallurgy*, Elsevier, Amsterdam **2015**.

[42] J. Mo, Z. Kang, G. Yang, S. T. Retterer, D. A. Cullen, T. J. Toops, J. B. Green, F.-Y. Zhang, *Appl. Energy* **2016**, *177*, 817.

[43] H. Li, T. Fujigaya, H. Nakajima, A. Inada, K. Ito, *J. Power Sources* **2016**, *332*, 16.

[44] S. Siracusano, A. Di Blasi, V. Baglio, G. Brunaccini, N. Briguglio, A. Stassi, R. Ornelas, E. Trifoni, V. Antonucci, A. S. Aricò, *Int. J. Hydrogen Energy* **2011**, *36*, 3333.

[45] M. Suermann, K. Takanohashi, A. Lamibrac, T. J. Schmidt, F. N. Büchi, *J. Electrochem. Soc.* **2017**, *164*, F973.

[46] J. K. Lee, G. Y. Lau, F. Shen, A. Bergeson-Keller, X. Peng, M. C. Tucker, *J. Electrochem. Soc.* **2024**, *171*, 64505.

[47] R. Lin, J. Huo, X. Cai, S. Lan, Z. Hao, *J. Power Sources* **2024**, *614*, 235030.

[48] T. Schuler, T. J. Schmidt, F. N. Büchi, *J. Electrochem. Soc.* **2019**, *166*, F555.

[49] M. F. Ernst, V. Meier, M. Kornherr, H. Gasteiger, *J. Electrochem. Soc.* **2024**, *171*, 74511.

[50] M. Bernt, C. Schramm, J. Schröter, C. Gebauer, C. Byrknes, C. Eickes, H. A. Gasteiger, *J. Electrochem. Soc.* **2021**, *168*, 84513.

[51] M. Bernt, H. A. Gasteiger, *J. Electrochem. Soc.* **2016**, *163*, F3179.

[52] C. Liu, M. Shviro, G. Bender, A. S. Gago, T. Morawietz, M. J. Dzara, I. Biswas, P. Gazdzicki, Z. Kang, S. F. Zaccarine, S. Pylypenko, K. A. Friedrich, M. Carmo, W. Lehnert, *J. Electrochem. Soc.* **2023**, *170*, 34508.

[53] A. A. Mazhar, F. E.-T. Heakal, A. G. Gad-Allah, *Corrosion* **1988**, *44*, 705.

[54] C. A. Schneider, W. S. Rasband, K. W. Eliceiri, *Nat. Methods* **2012**, *9*, 671.

[55] S. van der Walt, J. L. Schönberger, J. Nunez-Iglesias, F. Boulogne, J. D. Warner, N. Yager, E. Gouillart, T. Yu, *PeerJ* **2014**, *2*, e453.

[56] J. Gostick, Z. Khan, T. Tranter, M. Kok, M. Agnaou, M. Sadeghi, R. Jervis, *JOSS* **2019**, *4*, 1296.

[57] J. Landesfeind, J. Hattendorff, A. Ehrl, W. A. Wall, H. A. Gasteiger, *J. Electrochem. Soc.* **2016**, *163*, A1373.

[58] R. Makharia, M. F. Mathias, D. R. Baker, *J. Electrochem. Soc.* **2005**, *152*, A970.

[59] C. R. Harris, K. J. Millman, S. J. van der Walt, R. Gommers, P. Virtanen, D. Cournapeau, E. Wieser, J. Taylor, S. Berg, N. J. Smith, R. Kern, M. Picus, S. Hoyer, M. H. van Kerkwijk, M. Brett, A. Haldane, J. F. Del Río, M. Wiebe, P. Peterson, P. Gérard-Marchant, K. Sheppard, T. Reddy, W. Weckesser, H. Abbasi, C. Gohlke, T. E. Oliphant, *Nature* **2020**, *585*, 357.

[60] P. Virtanen, R. Gommers, T. E. Oliphant, M. Haberland, T. Reddy, D. Cournapeau, E. Burovski, P. Peterson, W. Weckesser, J. Bright, S. J. van der Walt, M. Brett, J. Wilson, K. J. Millman, N. Mayorov, A. R. J. Nelson, E. Jones, R. Kern, E. Larson, C. J. Carey, İ. Polat, Y. Feng, E. W. Moore, J. VanderPlas, D. Laxalde, J. Perktold, R. Cimrman, I. Henriksen, E. A. Quintero, C. R. Harris, et al., *Nat. Methods* **2020**, *17*, 261.

[61] The Pandas Development Team, pandas-dev/pandas: Pandas **2024**, https://doi.org/10.5281/zenodo.3509134.

[62] W. McKinney, in *Proc. 9th Python in Science Conf.* **2010**, p. 56.

[63] J. D. Hunter, *Comput. Sci. Eng.* **2007**, *9*, 90.

[64] M. Murbach, B. Gerwe, N. Dawson-Elli, L. Tsui, *JOSS* **2020**, *5*, 2349.

[65] K. Bobzin, *Oberflächentechnik Für Den Maschinenbau*, Wiley, Hoboken, NJ **2013**.